Three-Dimensional Aspects of Microwave Holography

Richard F. Schindel

Houston Advanced Research Center
4802 Research Forest Drive, The Woodlands, Texas, USA 77381 (713) 363-7922

ABSTRACT

Conventional active microwave imaging implies a synthetic aperture radar (SAR) range-Doppler processor. The range-Doppler processing is inherently two-dimensional. Resolution in the range dimension is obtained by processing transmitted bandwidth. Resolution in the cross-range dimension is obtained by processing the Doppler shift caused by relative motion between the transceiver and the target. Range and Doppler variables are assumed to be rectangularly orthogonal, hence the small angle limitation associated with conventional SAR. What is more important, these variables are the only dimensional information available using range-Doppler processing. Researchers have been working on three-dimensional SAR implementations. Most of the research is concentrated in the use of ancillary data. Ancillary data includes simple techniques using target shadowing, and more complex techniques such as monopulse radars and ISAR processing [Wehner, 1987]. In contrast microwave imaging using a holographic SAR processor is inherently three-dimensional. Holographic processing provides at least two techniques for recovering three-dimensional target information. These techniques are projection plane imaging and tomographic imaging. Neither of these techniques requires ancillary data to form the third dimension. The difference between traditional SAR and holographic SAR is the mapping of measurements into Fourier space. ISAR is comparable in this mapping, except ISAR relies on target motion in two dimensions to provide three-dimensional images. Holographic processing does not rely on cooperative target motion for three-dimensional resolution. This paper describes the theory required to implement both projection plane and tomographic signal processors. Two experiments are presented to illustrate the capabilities of each technique for three-dimensional imaging.

Key Words (Microwave Imaging, Three-Dimensional Imaging, Microwave Holography, Inverse Problems).

INTRODUCTION

Holographic SAR processing is approximately a Fourier transform operation [Mensa, 1984]. Measurements of the field scattered from a given scene are mapped into Fourier space according to the wavevectors associated with the transmitted and scattered fields. If measurements are made at an inclination angle outside (above) the plane of the target, and these measurements utilize azimuthal angular and frequency diversity, then three-dimensional target information is obtained. The Fourier contour is a truncated cone whose surface is filled with complex scattered field measurements [Langenberg, 1987]. The fact that this technique provides three-dimensional resolution from a single pass by the target is not reported in the literature. Experiments to date have provided for the projection of the measurement cone into the horizontal plane only [Chan and Farhat, 1981]. An example of the type of measurement and image provided by this projection is shown in figure 1. Projecting the Fourier contour onto the horizontal plane provides an annulus of measurements as shown in figure 1. The scattered field data occupying this annulus are then inverted using a two-dimensional inverse Fourier transform to obtain an image containing width and depth information about the target, as shown in the figure. However, the Fourier contour is just as easily projected into any of the three-principle planes containing the target. The image of the target can therefore be collapsed to give profiles containing height, width, and depth information. This imaging process will be referred to as projection plane imaging. The implication of this processing technique is that three-dimensional target information can be obtained from a single pass by the target. It must be noted that each image plane contains all the illuminated sources comprising the target. In other words, no single plane contains completely unique information. A full unique three-dimensional image of a target is possible using tomographic processing of three-dimensional measurements. Three-dimensional measurements can be obtained by synthesizing both azimuth and elevation angular apertures and trans-

mitting a frequency diverse waveform at each aperture position. Using all three diversity variables means that the scattered field measurements occupy the volume of the truncated cone in Fourier space. Thus, using the Fourier projection-slice theorem a full three-dimensional image of the target can be constructed.

To illustrate both three-dimensional processes, projection plane and tomographic imaging, two basic laboratory experiments are presented. The first experiment reported is designed to investigate the projection plane processing technique. Measurements and images of a simple target consisting of several discrete scatterers illustrate the collapsing of the Fourier contour into multiple planes, as well as the three-dimensional information content of the reconstructed projection images. The more well known tomographic processing is illustrated by a second laboratory experiment in which a dielectric cone with simple internal structure is reconstructed in several tomographic slices. To contrast projection plane imaging with tomographic imaging, projection images of the cone target are also included.

Both types of three-dimensional imaging techniques have application in medical diagnostics, as well as, in environmental remote sensing and military target classification. Tomographic processing is most popular with medical and non-destructive evaluation applications. These applications can accommodate the effort required to obtain large three-dimensional data sets. Multi-plane holographic projection imaging has not been fielded. However the most important applications of the technique will be environmental remote sensing and military target classification. For these applications single passes over the target area are more desirable due to the cost and risk involved in multiple passes or multiple platforms for data acquisition.

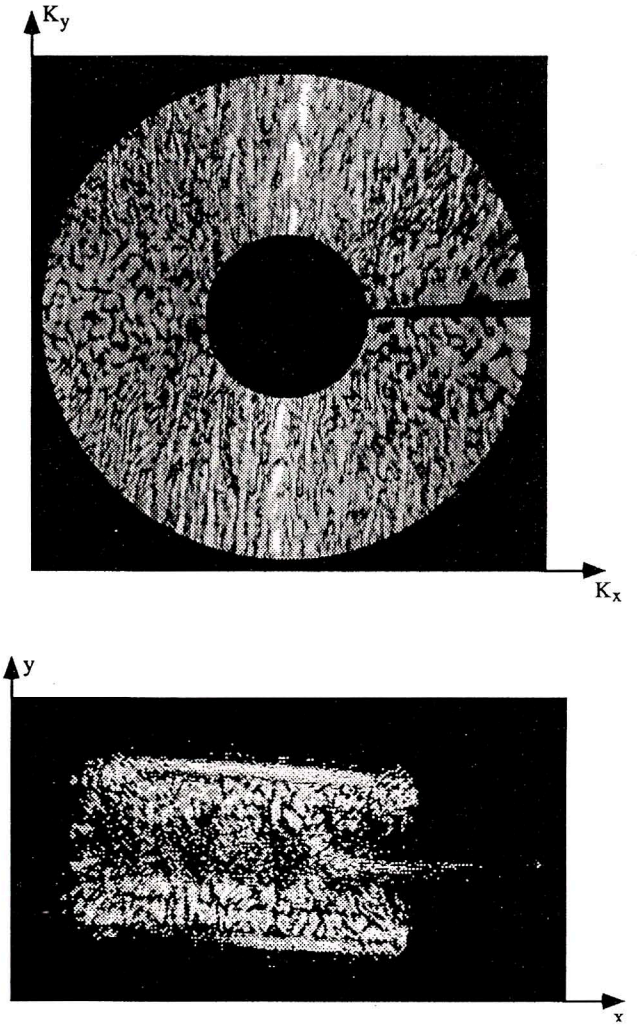

Fig. 1 - Typical Fourier annulus projection and corresponding image formed using a holographic SAR processor.

1. THEORY

The far-field microwave inversion algorithm known as holographic SAR relates, within the Born approximation, the target scattering function to the inverse Fourier transform of the phase normalized scattered field. To within a constant, and assuming target scattering properties are essentially constant with respect to frequency, the scalar version of the algorithm for plane wave excitation can be written as [Langenberg, 1987]:

$$O_{LP}(\bar{R}) = F_{3D}^{-1}\left\{\Phi_s^{far}(\bar{K})\, e^{jkR}\right\} \qquad (1)$$

where $\Phi_s^{far}(\bar{K})$ is the scattered far-field, $O_{LP}(\bar{R})$ is the function associated with the scattering function of the target, $\bar{R}$ and $\bar{K}$ are the Fourier variable pair, k is the incident wavenumber, and R is the distance between the transmitter and the phase reference point. The phase reference point is an arbitrarily positioned point at which the phase of the incident field is known. Conventional experiments generally establish the phase reference at the center of the target through a calibration measurement. The scattering function, $O_{LP}(\bar{R})$ is a low pass filtered version of a function describing many scattering mechanisms. This function has been reported as an object function [DeVaney, 1980], and a reflectivity function [Mensa, 1984]. The object function is a mathematical abstraction that is described as a Kronecker Delta type of function used to describe the shape of the target. Clearly this does not provide a true physical description of the inversion process. Neither is the description as a reflectivity function adequate to describe the physical inversion process.

The nature of the function is a complicated combination of reflectivity, edge scattering, creeping wave reflections, and source interactions. This scattering function is the end goal of the inversion process. A magnitude or intensity plot of this function provides the image of the target. The scattered far-field provides the starting point for the mathematical inversion in (1). As indicated in (1), the measurement process used to obtain the scattered field can be considered a Fourier space process. The magnitude of the Fourier vector is dependent on the wavelength of illumination. The direction of the Fourier vector when considering far-field measurements is determined by the relative angular positions of the transmitter and receiver antennas. The antenna positions give the propagation directions of the primary and scattered wavefronts. The Fourier vector associated with the measurement process is therefore represented by:

$$\bar{K} = k\left(\hat{R}_r + \hat{R}_t\right) \qquad (2)$$

where $\hat{R}_r$ is the unit vector in the receive direction and $\hat{R}_t$ is the unit vector in the transmit direction. The properties of the Fourier vector determine how scattered field measurements are mapped into Fourier space. This mapping determines the properties of the image.

Two measurement parameters available to manipulate the Fourier vector are the illumination wavelength, and the angle between the transceiver and target. From (2), the angle of the Fourier vector is determined from the position of the transmit antenna and the receive antenna. To describe the behavior of the Fourier vector, the general measurement geometry of figure 2 is used. In figure 2, the transmit antenna and the receive antenna are positionally independent, and can be placed at, and moved through, any azimuth or elevation position. The choice of coordinate system is arbitrary; but for simplicity, the origin is placed at the center of the target scene. The sequence of azimuth and elevation angles at which measurements are made is completely arbitrary, as is the sequence in which frequencies are transmitted at each angular position. To provide a tractable, yet general, example of Fourier mapping, a few assumptions are made. First, it is assumed that measurements are made at several azimuth angles surrounding a target before moving to another elevation angle and repeating the azimuth scan. It is further assumed that only elevation angles above the xy-plane are available. For constant wavelength illumination, Fourier space will be filled according to the map of figure 3. As indicated in part (a) of the figure, each azimuth scan results in a circle parallel to the KxKy-plane. Part (b) of the figure indicates that the placement of each circle along the Kz-axis is determined by the elevation angle. The elevation angle also determines the radius of the circle in the KxKy-plane.

By employing two-dimensional angular diversity, the surface of the Ewald sphere associated with the wavelength of illumination is filled with data. The choice of azimuth angles and elevation angles determines what the contours on this spherical surface will look like.

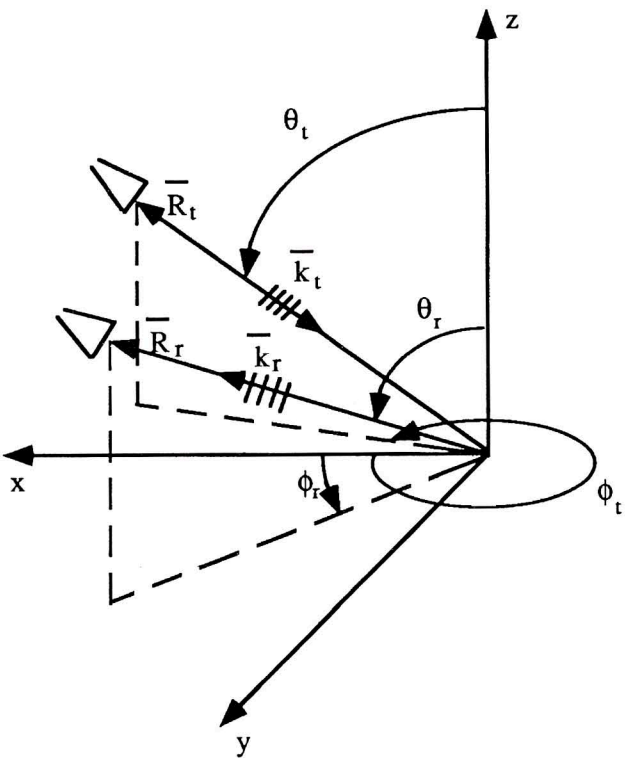

Fig. 2 - Generalized geometry for holographic recording. θ_r and Φ_r are the elevation and azimuth angles corresponding to the transmit antenna, θ_t and Φ_t are the elevation and azimuth angles corresponding to the receive antenna, $\bar{R}_t$ and $\bar{R}_r$ are the radius vectors to the transmit and receive antennas respectively, $\bar{k}_t$ and $\bar{k}_r$ are the transmitted and scattered wavevectors, respectively.

The contours shown in figure 3 will have the same shape for either monostatic or fixed angle bistatic configurations. However, for monostatic, the angle of the Fourier vector for any given measurements point is equal to the receive position angle. For bistatic configurations, the angle of the Fourier vector is the bisector of the angle between the transmitter and receiver. The contours of figure 3 assume that the transmit and receive platforms move in tandem. This, of course, is always true for monostatic measurements, but multi-platform configurations where this is not true are possible. These cases will be referred to as multistatic configurations. Of significant interest is a scenario where the transmitter is fixed with respect to the target, and the receiver is free to move about the target to form the measurement aperture. Since the transmitter is constantly illuminating the target from a

single angle, only a single set of scattering sources supported by the target is active. For the monostatic and fixed angle bistatic configurations, the image results from an angular average of scattering sources. From (2) it is clear that multistatic measurement contours in Fourier space will be different from those shown in figure 3. Figure 4 contains a plot of the multistatic angular diverse Fourier contours. The contours are no longer concentric, but tangent at the point where the transmit antenna and the receive antenna are spatially separated by 180 degrees in azimuth. The Fourier space available with the receiver rotation configuration is exactly half that available for the monostatic configuration.

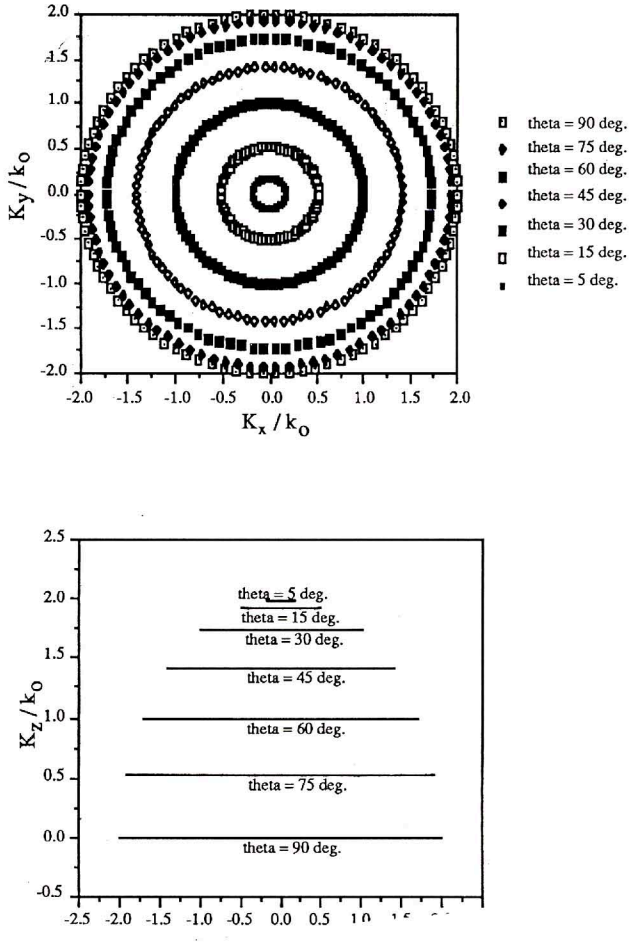

Fig. 3 - Monostatic and fixed angle bistatic Fourier mapping. The components of the Fourier vector are normalized to the maximum transmitted wavevector k_0 . (a) KxKy-plane Fourier contours corresponding to azimuth over elevation object rotation; (b) location of KxKy-planes along the rotation axis.

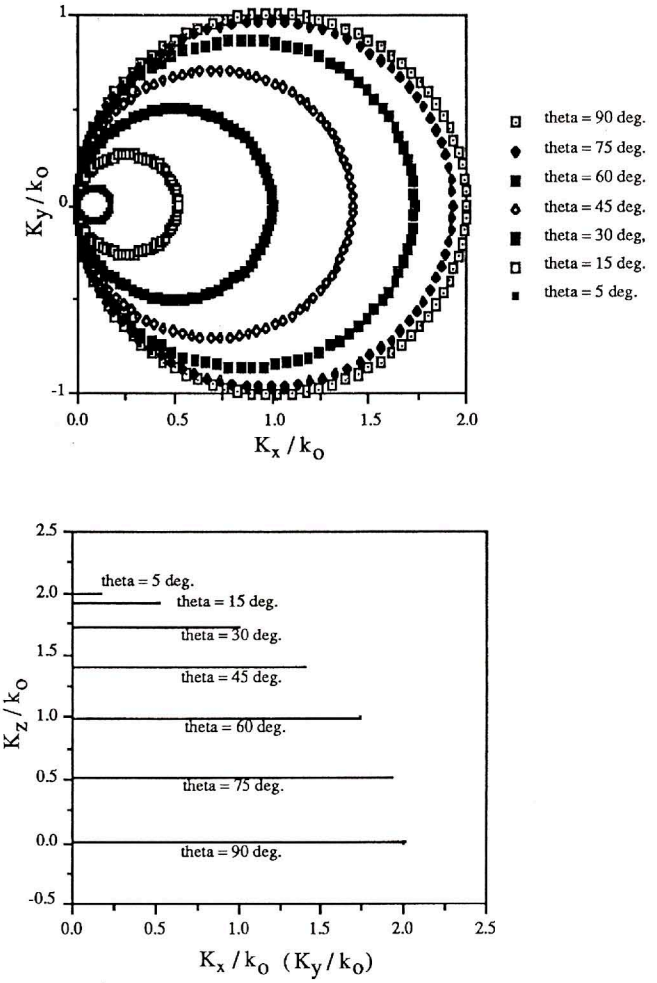

Fig. 4 - Multistatic Fourier mapping. The components of the Fourier vector are normalized to the maximum transmitted wavenumber, k_0 . (a) KxKy-plane Fourier contours corresponding to azimuth over elevation receiver rotation; (b) location of KxKy- planes along the rotation axis.

It is possible to acquire sufficient data for imaging through angular diversity alone. However, it is far more efficient to use a combination of angular and frequency diversity. Frequency diversity provides range resolution in SAR processors, and serves the same function in holographic processors. The relationship between the frequency of illumination, and the magnitude of the Fourier vector is linear. As the illumination wavelength is varied, the radius of the Ewald sphere is varied. Frequency diversity has no effect on the direction of the Fourier vector, and therefore exhibits the same behavior regardless of the antenna configuration. Figure 5 contains a plot of frequency diverse Fourier space with a parameter of elevation angle. The scenario in the figure assumes a uniformly sampled

waveform, which results in uniform sampling along the Fourier contour. However, with adequate sampling, any waveform can be used with the processor. The elevation angle serves to change the slope of the frequency line. Note that an elevation angle of ninety degrees, with respect to the vertical, results in a horizontal line. If the elevation angle is kept constant at an angle different from ninety degrees, and an azimuth only aperture is synthesized, then the Fourier contour can be represented by the truncated cones in figure 6. Part (a) of the figure represents the Fourier surface for monostatic [Langenberg, 1987] and fixed angle bistatic configurations, and part (b) of the figure represents the Fourier surface for a multistatic configuration.

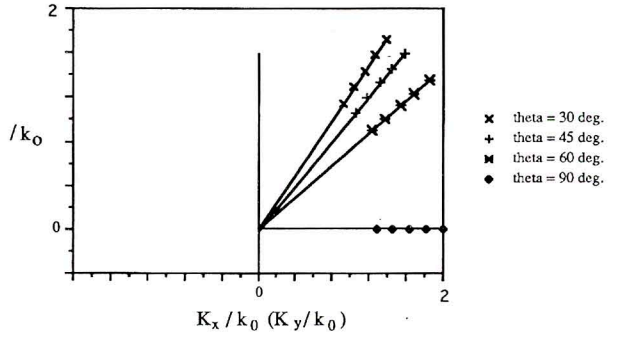

Fig. 5 - Frequency map of Fourier space for several Fourier elevation angles, theta. The components of the Fourier vector are normalized to the maximum transmitted wavenumber, k_0.

To form the measurement surfaces of figure 6, two degrees of freedom are required of the measurement configuration. However, the resulting contour has spatial frequency extent in each of the three Fourier dimensions. This implies resolution in each of the three spatial dimensions. It is traditional that images are formed in the xy-plane [Chan and Farhat, 1981, Mensa, 1984, Schindel, 1989]. To accomplish the inversion, either the measurements are made using a waterline configuration [DeVaney 1981, Mensa, 1984], or the measurement contour is projected to an annulus in the KxKy-plane [Chan and Farhat, 1981]. To project the contour into the elevation planes, x=0 and y=0, requires no more computational effort than projection into the z=0 plane. As long as the measurements are made at an elevation plane other than the z=0 plane, the target can be resolved in each of the planes. An example of the projection of a monostatic contour into the three principle planes is shown in figure 7. The azimuthal measurement

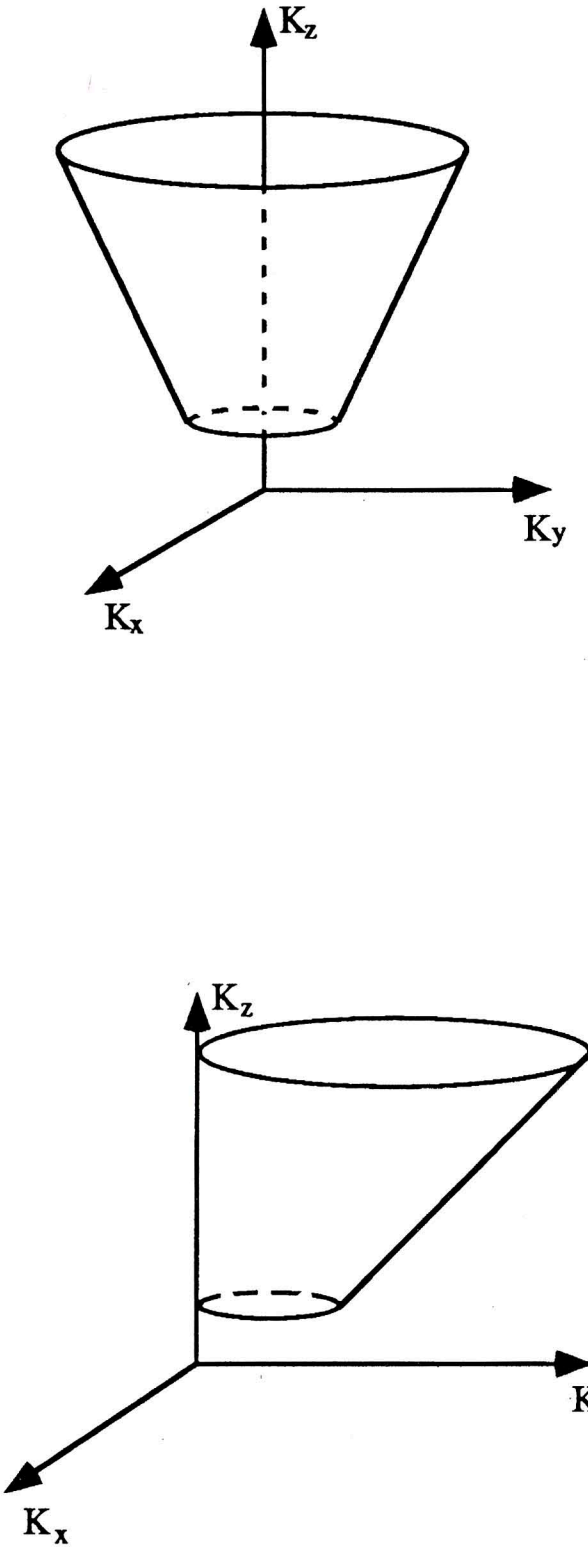

Fig. 6 - Two degree-of-freedom measurement aperture obtained using frequency diversity and full coverage azimuthal angular diversity at a constant elevation. (a) monostatic and fixed angle bistatic surface; (b) multistatic surface.

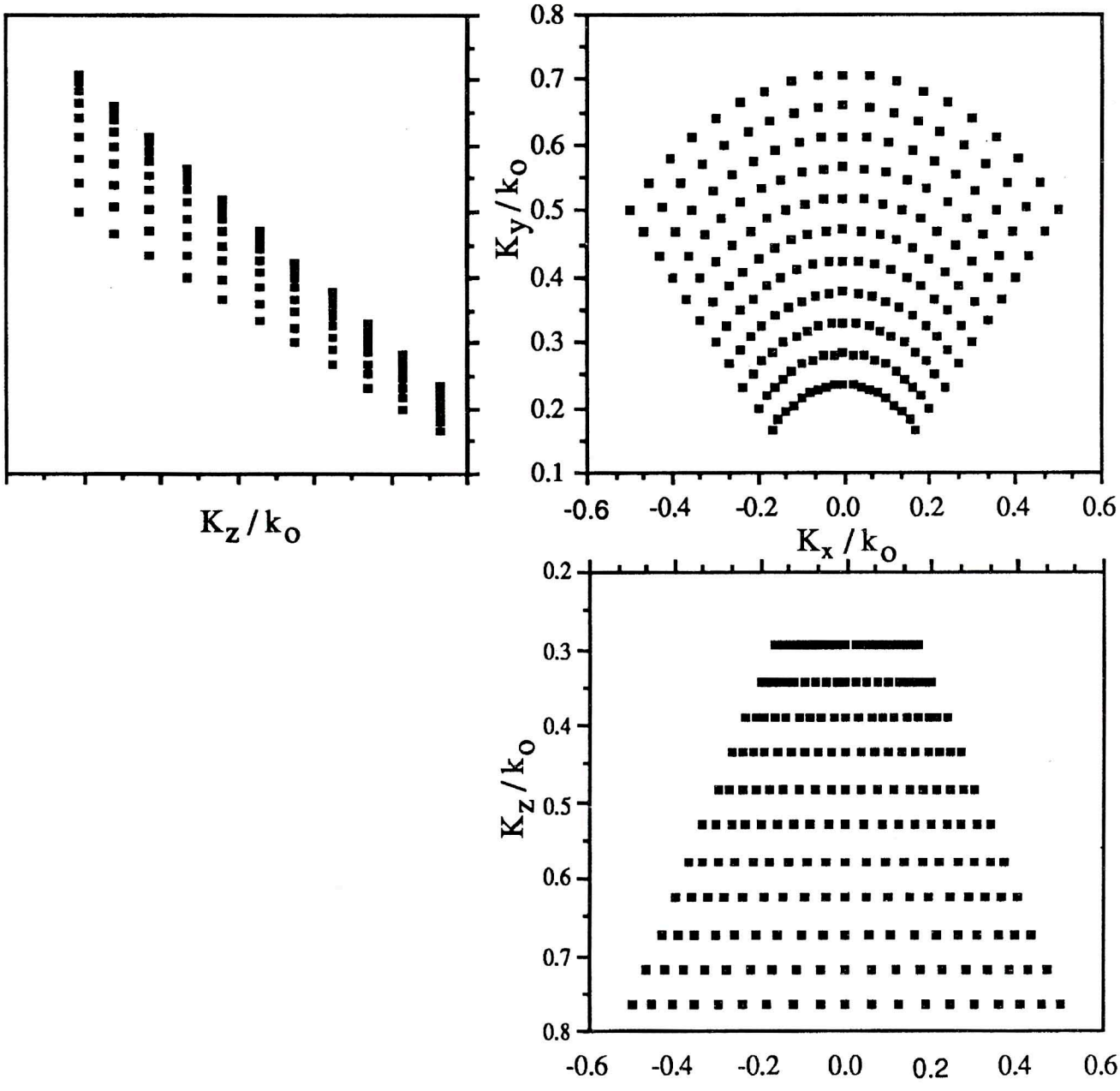

Fig. 7 - Projection of a partial coverage two degree-of freedom-measurement aperture into the three principle Fourier space planes. Components of the Fourier vector are normalized to the maximum transmitted wavenumber, k_0.

aperture is synthesized over a ninety degree azimuth aperture, which is symmetrical about the x-axis. The elevation of the antenna is forty-five degrees. Projection of the truncated cone into the xy aperture gives the conventional truncated annulus area. Projection of the cone into the xz-plane maps as a trapezoid area with ninety degrees of aperture. Projection of the contour into the yz-plane results in a much smaller angular aperture. This will result in an xy-plane image with relatively poor resolution in the track dimension. Processing these three orthogonal planes gives plan and elevation views of the target.

Multiple projection plane images will provide three-dimensional information about the target from a single pass measurement set. However, each of the images formed from the Fourier map of figure 7 will contain all of the measured scattering information. No single plane contains unique information. To obtain unique three-dimensional information about the target, a true three-dimensional volume of Fourier space must be filled with measurements. This requires the use of both azimuth and elevation angular diversity and frequency diversity. The volume of Fourier space filled with data can be visualized by com-

bining the components of diversity illustrated in figures 3(a) and 5. Figure 5 depicts frequency diversity and elevation angular diversity. Adding the azimuthal angular diversity of figure 3(a) has the effect of rotating the plot of figure 5 about the Kz axis. This rotation has the effect of filling several concentric conical surfaces of figure 6(a). The volume occupied by these concentric cones is shown in figure 8. Since three-dimensions are employed in the measurement schemes, the measurement volume has finite spatial frequency bandwidth in all three dimensions. Therefore, true resolution is obtained in all three spatial dimensions.

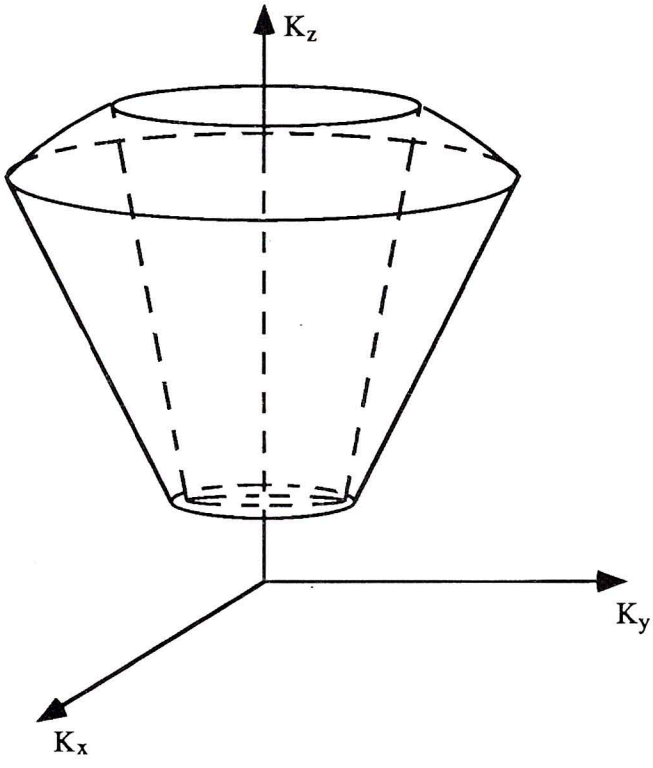

Fig. 8 - Three-dimensional spectral measurement volume obtained using two-dimensional monostatic angular diversity combined with frequency diversity.

Once measurements made with the three degrees-of-freedom are available, it is possible to reconstruct the entire three-dimensional distribution of scattering sources residing within the volume of the scattering object. The reconstruction may be accomplished using a three-dimensional FFT. However, it is generally not possible to view the entire three-dimensional structure of the reconstructed sources in an easily interpretable fashion. This is especially true of penetrable scatterers. A three-dimensional secondary source distribution requires four dimensions of the plotting apparatus. This problem can be overcome through the use of tomography. Tomographic processing is used to generate two-dimensional slices, called tomograms, of the reconstructed three-dimensional scattering sources [Ramachandran and Lakshminarayanan, 1971]. The entire three-dimensional reconstruction consists of a series of these tomograms. Tomography is based on the Fourier projection-slice theorem [Radon, 1917]. This theorem states that the inverse Fourier transform of an N-1 dimensional projection, of an N dimensional Fourier transformed function, yields a slice of the function in object space. The theorem is easily derived starting with the three-dimensional secondary source function. If the function p(x,y,z=b) is taken as the z=b plane slice of the three-dimensional secondary source function, then mathematically the slice can be selected using a two-dimensional Dirac delta function, as shown by:

$$p(x,y,z=\beta) = p_{z=\beta}(x,y) = \int_{-\infty}^{\infty} p(x,y,z)\,\delta(\beta - z)\,dz \tag{3}$$

where $p_{z=\beta}(x,y)$ is shorthand notation for the slice of the three-dimensional sources contained the $z = \beta$ plane. Substitution of (3) into the three-dimensional Fourier transform of (1), yields the projection slice theorem in the form shown below:

$$p_{z=\beta}(x,y) = F_{2D}^{-1}\left\{P_{z=\beta}\left(K_x, K_y\right)\right\} \tag{4}$$

where the Fourier domain projection is given by the integral equation:

$$P_{z=\beta}\left(K_x, K_y\right) = \int_{-\infty}^{\infty} P\left(K_x, K_y, K_z\right) e^{j(K_z\beta)}\,dK_z \tag{5}$$

Equation (5) weights each of the measurements in all of the Kz-planes of figure 8 according to the indicated exponential phase term, and integrates the resulting filtered measurements over all recorded Kz planes. The physical interpretation of the projection slice theorem is that of propagating plane waves of wave vector Kz in the z-direction by an amount β . The plane waves are then added coherently to form the projected two-dimensional secondary source spectrum. This spectrum is inverted using the two-dimensional version of the algorithm to obtain the slice $z = \beta$ of the scattering function. Unlike the projection imaging process, the tomogram is a unique representation of the scatterers occupying the $z = \beta$ plane. No out of plane sources are projected into the tomogram. To fully reconstruct the scattering function, the process must be carried out for several values of β . From an operational point of view, this may be restrictive for field measurements since several passes over the target area are necessary to acquire the volume of data required for tomographic reconstruction.

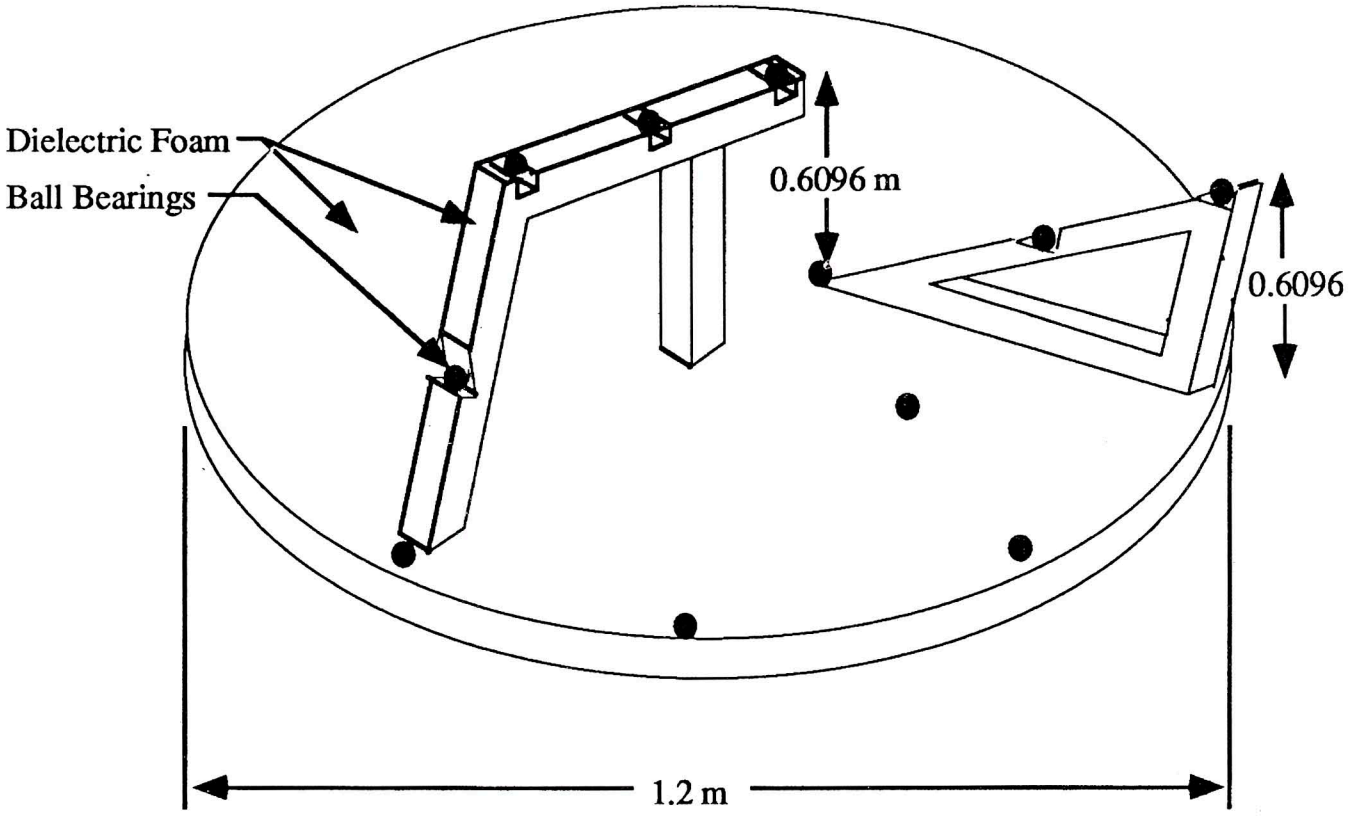

Fig. 9 - Schematic representation of the target used to verify three-dimensional projection plane imaging.

2. EXPERIMENTAL EVIDENCE

Microwave holography offers two types of three-dimensional imaging to be performed. These are projection images and tomographic images. To demonstrate each of these processes, two experiments are presented. Both experiments are performed using a monostatic measurement configuration, but the method is equally applicable to fixed angle bistatic measurements and multistatic measurements. The first experiment is designed to verify the projection plane imaging process, and indicate the information obtained from projection images. The second experiment illustrates the tomographic reconstruction of scattering sources supported by a target. Projection images of the target are presented for comparison of the two techniques.

To demonstrate the capabilities for three-dimensional projection plane imaging, a simple target is used. This target consists of stainless steel ball bearing scatterers placed in a three-dimensional pattern on a dielectric foam support. The target is shown schematically in figure 9. The ball bearings are placed in a manner which provides a different pattern of scatterers in each of three principle projection planes. Scatterer placement is shown in figure 10. As shown in the figure, the scatterers form a pie slice shape in the xy-plane, a distorted rectangle in the xz-plane, and a forty-five degree right triangle in the yz-plane. These patterns allow easy verification of the three-dimensional capabilities of microwave holography. Specifically, the theory indicates that as long as the transmit and receive antennas do not lie in the same elevation plane as the target, then resolution is obtained in three-dimensions from a single angular sweep of the target. The experiment is designed for large scene size, high resolution, and more than four times oversampling. Experimental parameters are listed in table 1. The target is placed on a rotating pedestal so that the scatterers will reside in the proper planes, as shown in figure 10. The experiments provides for high resolution in the xy- and xz-planes, but extremely poor resolution is obtained in the yz-plane. Figure 11 contains the magnitude of the Fourier mapped hologram for the experiment described in table 1. Figure 12 contains the reconstructed images. Scatterers lying in the xy-plane appear slightly defocused in the image. This is due to a misalignment of the calibration target and the discrete target. Scatterers associated with the xz-plane are focused. The defocused source appearing in the image of this target plane is the projection of one of the scatterers lying outside the target plane. The images also contain clutter associated with the foam base and bearing supports. The position of the scatterers is consistent with the target in both the xy-

and xz-plane images. The geometric patterns are consistent with those indicated in figure 10 verifying resolution in both plan and elevation images. As indicated by the Fourier space plots, resolution in the yz-plane is very poor in the track dimension due to the small angular aperture. Resolution in the cross-track dimension is equal to that of the other images since resolution in this dimension is primarily due to bandwidth.

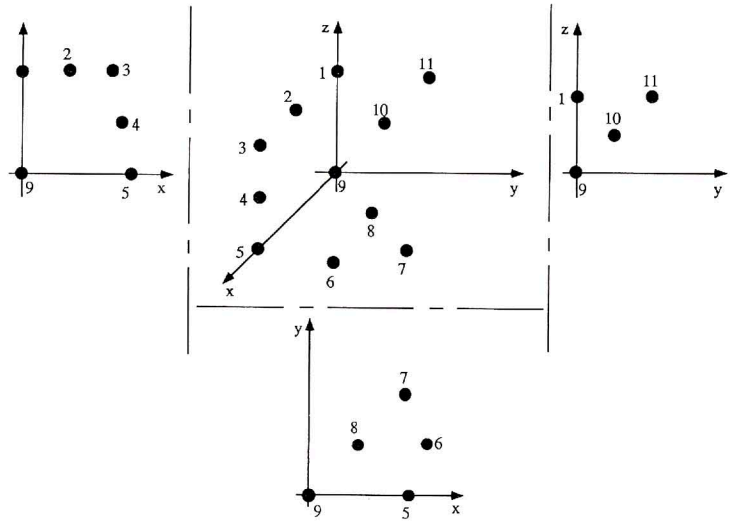

Fig. 10 - Three-dimensional positions of the ball bearing scatterers comprising the target of figure 9.

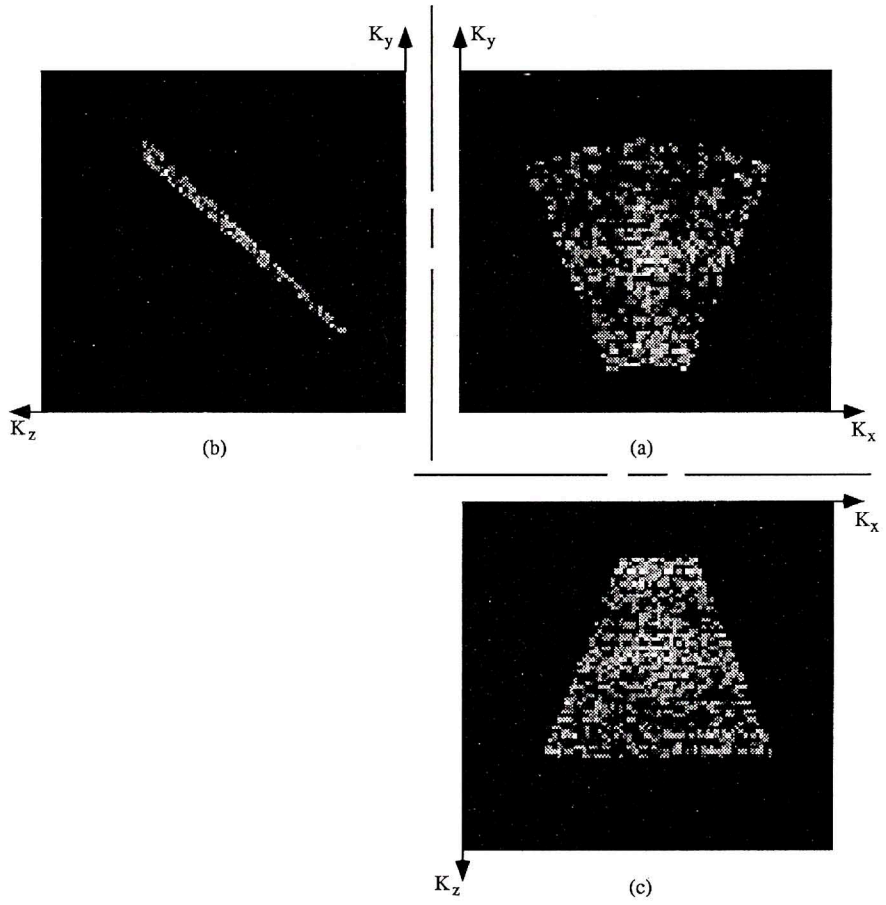

Fig. 11 - Magnitude of the Fourier mapped measurements for the discrete scatterer target. (a) KxKy-plane data; (b) KyKz-plane data; (c) KxKz-plane data.

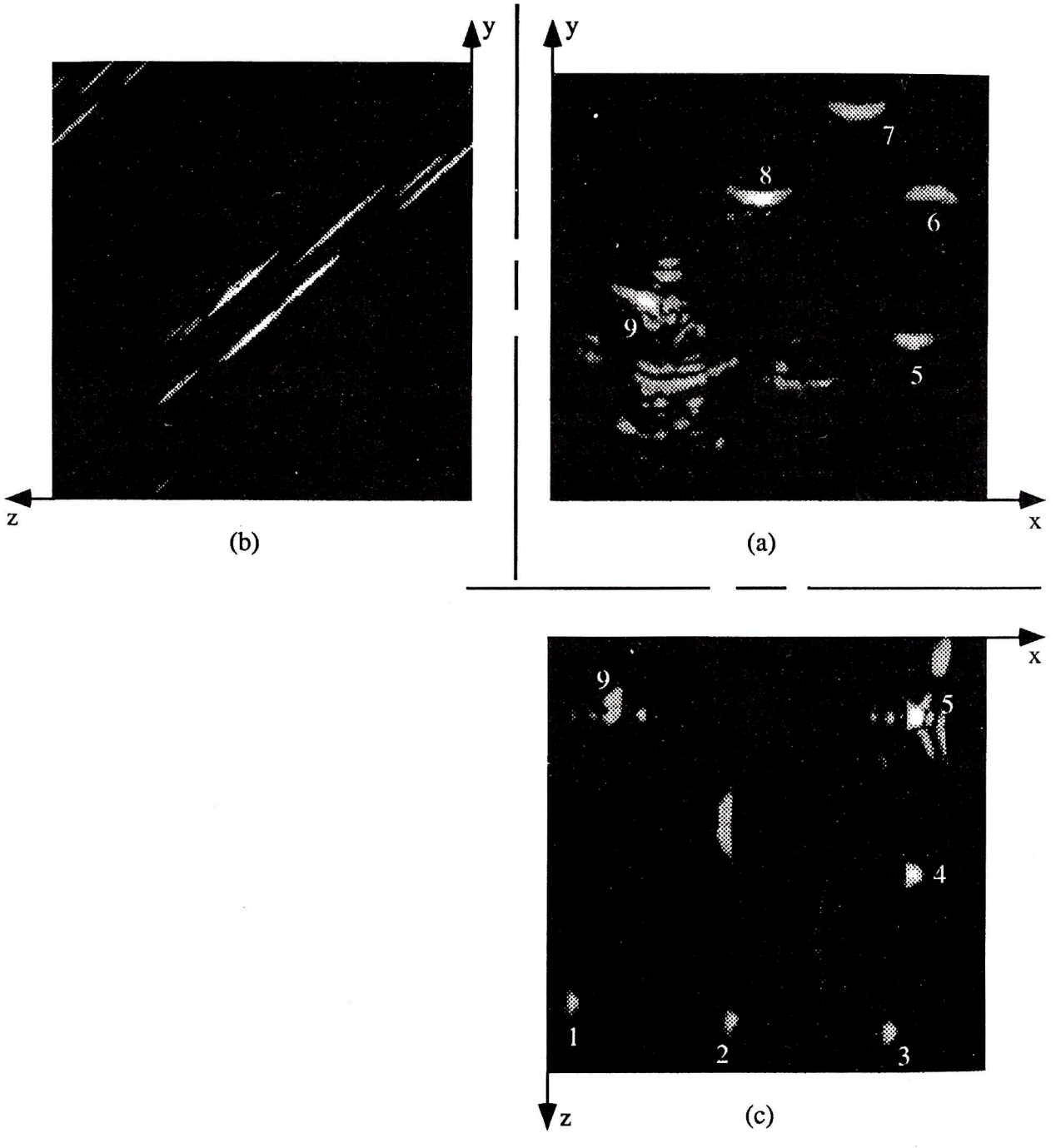

Fig. 12 - Projection plane images of the discrete scatterer target. The numbers correspond to the scatterer positions shown in figure 10. (a) xy-plane image; (b) yz-plane image; (c) xz-plane image.

The defocusing of these out-of-plane scatterers produced the idea of being able to refocus the image. Depth of focus, a traditional figure of merit for SAR sensors, is dependent on the resolution of the sensor [Wehner 1987]. As shown in table 1, the experiment design provides for a resolution cell on the order of 0.75 cm. Since the physical extent of the target is much greater than the resolution cell size, scatterers outside the principle focal plane (depth of focus) of the processor appear blurred. The capability of spatially adjusting the focal plane has been built into the processor, allowing the processor to move the plane of principle focus along an axis perpendicular to the plane containing the image. This capability works by modifying the phase of the measured data according to the thin lens transfor-

mation [Goodman, 1968]. The refocused measurements are then processed normally. An example of the refocusing capability is shown in figure 13. The data has been refocused so that the principle focal plane is parallel to the xy-plane and shifted along the positive z-axis by 0.6096 m. This places the focal plane at the top of the target of figure 10. Scatterers 1,2,3, and 11 of figure 10 are reproduced in the refocused image. The remaining artifacts in the reconstruction result from the projection of out-of-plane scatterers. This refocusing capability provides further indications that even a single pass by the target can produce three-dimensional information without using ancillary data such as shadow length.

Table 1. Design parameters and image characteristics for the discrete target experiment.

DESIRED PARAMETERS:			
Angular Aperture		**Degrees**	**Radians**
	Increment	0.2500	0.0044
	Incident	43.5000	0.7592
Resolution		**Inches**	**Centimeters**
	Track	0.7500	1.9050
	Cross-track	0.7500	1.9050
		GHz	**Hz**
Start Frequency		6.0000	6.0000E+09
REQUIRED PARAMETERS:			
Frequency		**GHz**	**Hz**
	Bandwidth	11.3931	1.1393E+10
	Increment	0.0568	5.6767E+07
	Maximum	17.3931	1.7393E+10
	# of Samples	201	201
Wavelength		**Inches**	**Centimeters**
	Average	1.0057	2.5546
Angles		**Degrees**	**Radians**
	Aperture	42.11	0.7349
	Increment	0.1870	0.0033
	# of Samples	226	226
IMAGE CHARACTERISTICS:			
		Feet	**Meters**
Scene Size		12.54	3.8233
Resolution		**Inches**	**Centimeters**
	Track	0.7500	1.9050
	Cross-track	0.7500	1.9050

The discrete target experiment provides experimental verification of the three-dimensional projection plane imaging capabilities of microwave holography. From an operational standpoint, projection plane imaging is highly desirable because it requires a single angular scan of the target scene. The disadvantage of projection plane imaging is that all the scatterers comprising the image appear in each projection plane. This is evidenced in the images contained in figures 12 and 13, where the out-of-plane scatterers are defocused artifacts in each of the projections. This disadvantage can be overcome by tomographic processing. As discussed in the theory, tomographic processing provides true three-dimensional imaging capability. Only scatterers contained in the plane of interest are reproduced in the image. The disadvantage to tomographic processing is that the processor requires a true three-dimensional data set. From an operational point of view, this requirement amounts to several angular sweeps of the target at different elevation planes.

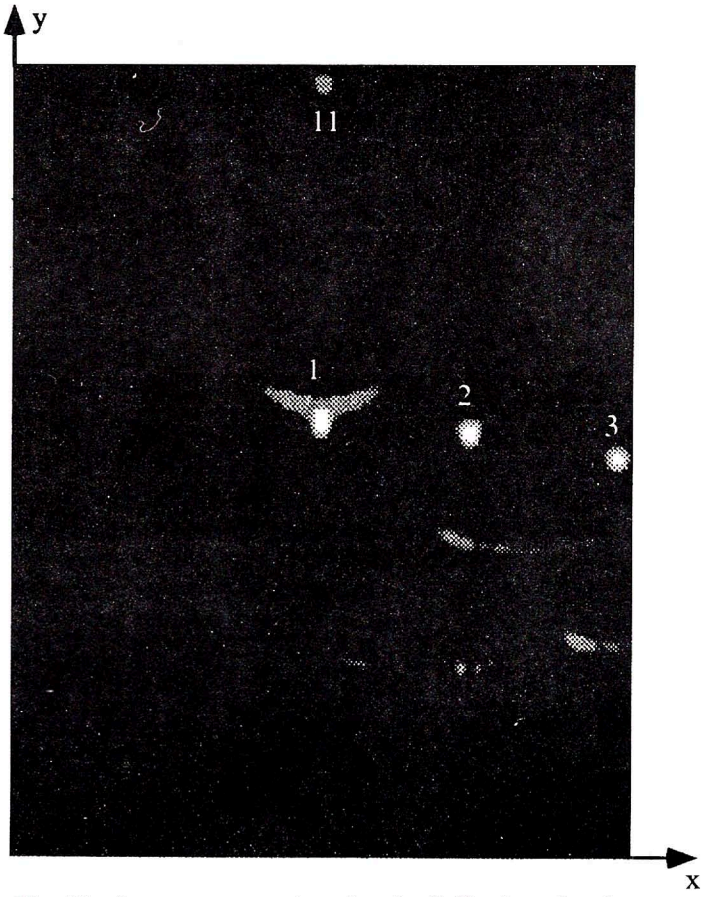

Fig. 13 - Image reconstruction after the KxKy-plane data has been refocused to the z=0.6096 meters plane. The numbers correspond to the scatterer positions shown in figure 10.

To illustrate the tomographic processor, the target of figure 14 is used, and a full three-dimensional data set is acquired. The experiment parameters are shown in table 2. The cone is made of dielectric foam, and has a sphere milled out of its center. The conical shape of the target provides a different cross-section for every tomogram along the axis of the cone. The spherical void provides internal structure to allow the investigation of target penetration. Figure 15 indicates the position of the tomograms presented in figure 16. Parts (b) and (c) of figure 15 show tomograms above and below the cone target to show that no sources associated with the cone appear outside the target volume. The sources indicated in part (c) of the figure are correlated with the target support structure. From figure 16, it is apparent that the tomographic processor is reconstructing only scattering sources which actu-

Table 2. Design parameters and image characteristics for the dielectric cone experiment.

MEASUREMENT PARAMETERS:					
Frequency		GHz	Hz		
	Bandwidth	14.00	1.40E+10		
	Increment	0.07	7.00E+07		
	Maximum	18.00	1.80E+10		
	# of Samples	201	201		
Wavelength		Inches	Centimeters		
	Average	1.07	2.72		
		AZIMUTH PLANE		ELEVATION PLANE	
Angles		Degrees	Radians	Degrees	Radians
	Aperture	180.00	3.14	90.00	1.57
	Increment	0.50	0.01	0.50	0.01
	# of Samples	361.00	361.00	181.00	181.00
IMAGE CHARACTERISTICS:		HORIZONTAL PLANE		ELEVATION PLANE	
		Feet	Meters	Feet	Meters
Scene Size		7.00	2.1343	7.00	2.1343
Resolution		Inches	Centimeters	Inches	Centimeters
	Track	0.4201	1.0671	0.4201	1.0671
	Cross-track	0.5347	1.3582	1.0694	2.7164

ally lie in the plane of interest. Due to the linearization approximation required for inversion, only the first-order scattering sources are visible [Wang and Chew, 1989]. The first-order scattering sources are the edge of the cone, and the spherical void, as well as, the standing waves supported by the dielectric-air interface in the void. Only half of the cone appears in any of the tomograms. This is due to the fact that a 180 azimuthal aperture was synthesized during the measurement process. Part (f) of figure 16 contains the tomogram coincident with the base of the cone. There are some scatterers visible in the center of the image. These scatterers correspond to the structure used to support the cone target during the experiment. For comparison purposes, plan view and elevation view projection images of the cone target are shown in figure 17. These image are obtained by processing the azimuth scan acquired when the antennas are located at an elevation of forty-five degrees. These projection images contain all of the sources supported by the target.

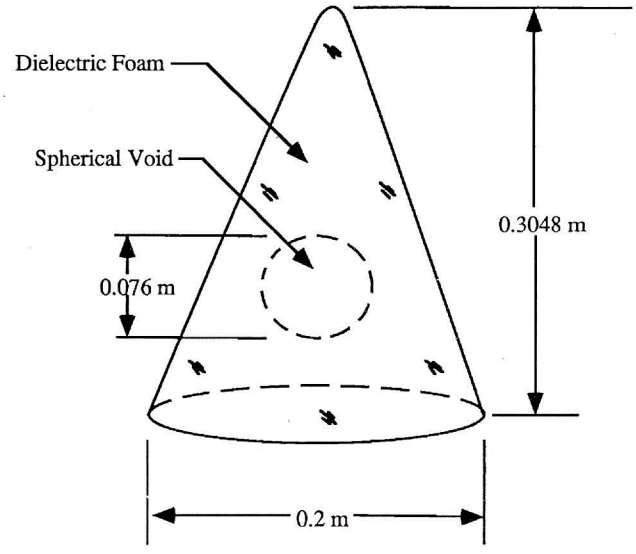

Fig. 14 - Schematic representation of the target used for verification of the tomographic capabilities of microwave holography.

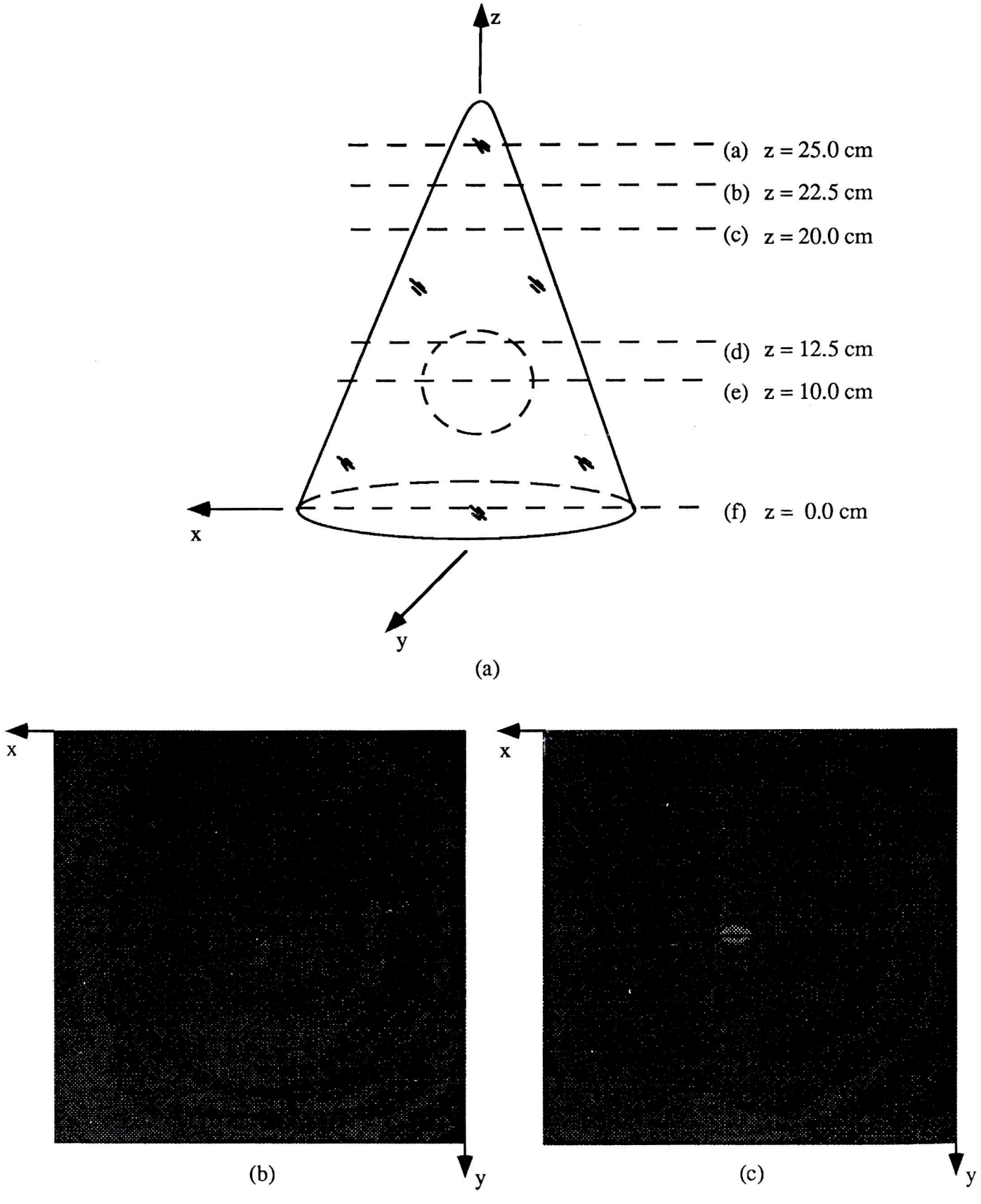

Fig. 15 - Relative location of the tomograms presented in figure 16. Parts (b) and (c) depict tomograms above and below the cone. Sources present in (c) are due to a support rod used to fix the cone to the rotating pedestal.

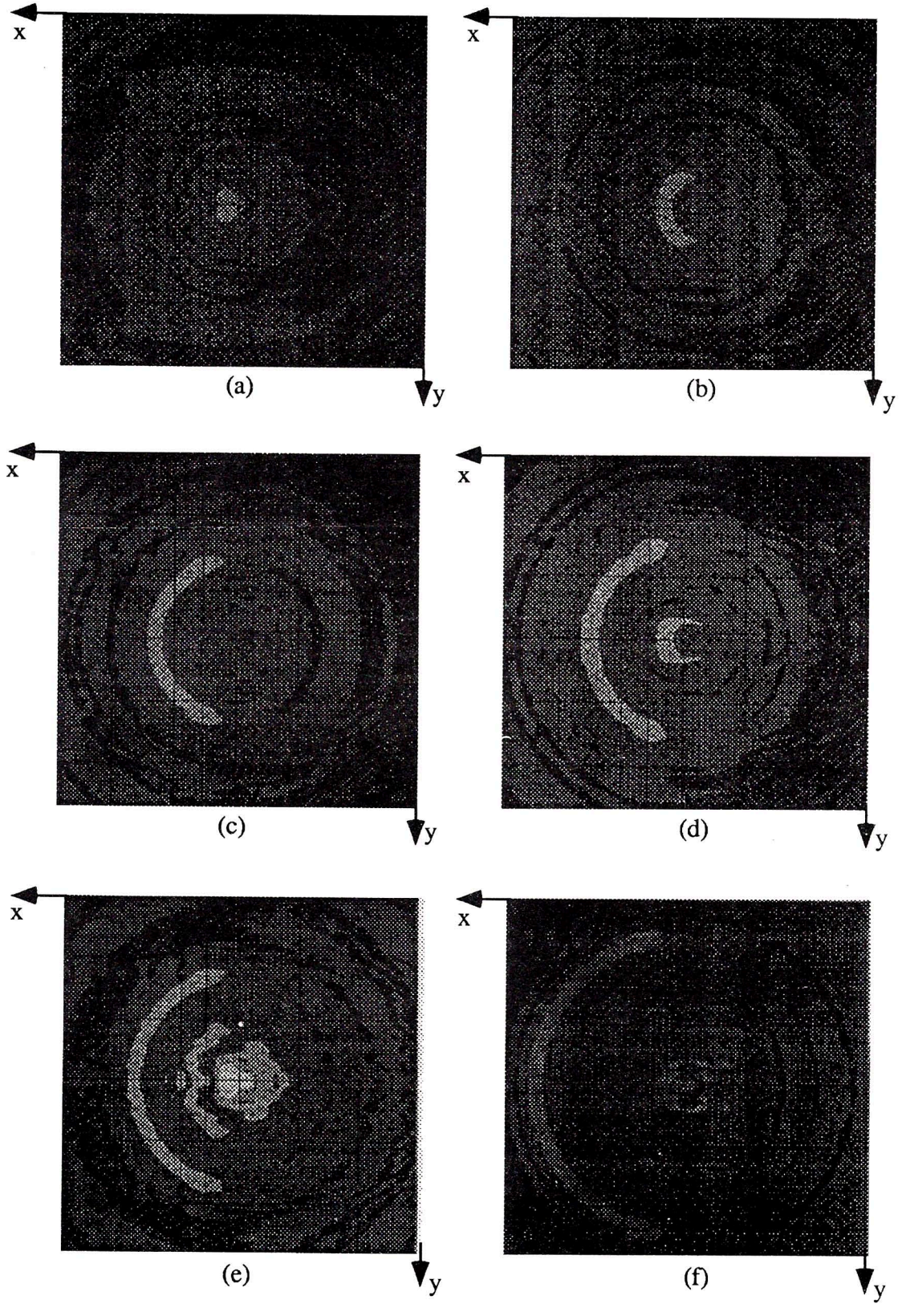

Fig. 16 - Tomographic reconstruction of the dielectric cone target. Parts (a) through (e) correspond to images of sources lying in the planes indicated by (a) through (e) lines in figure 15.

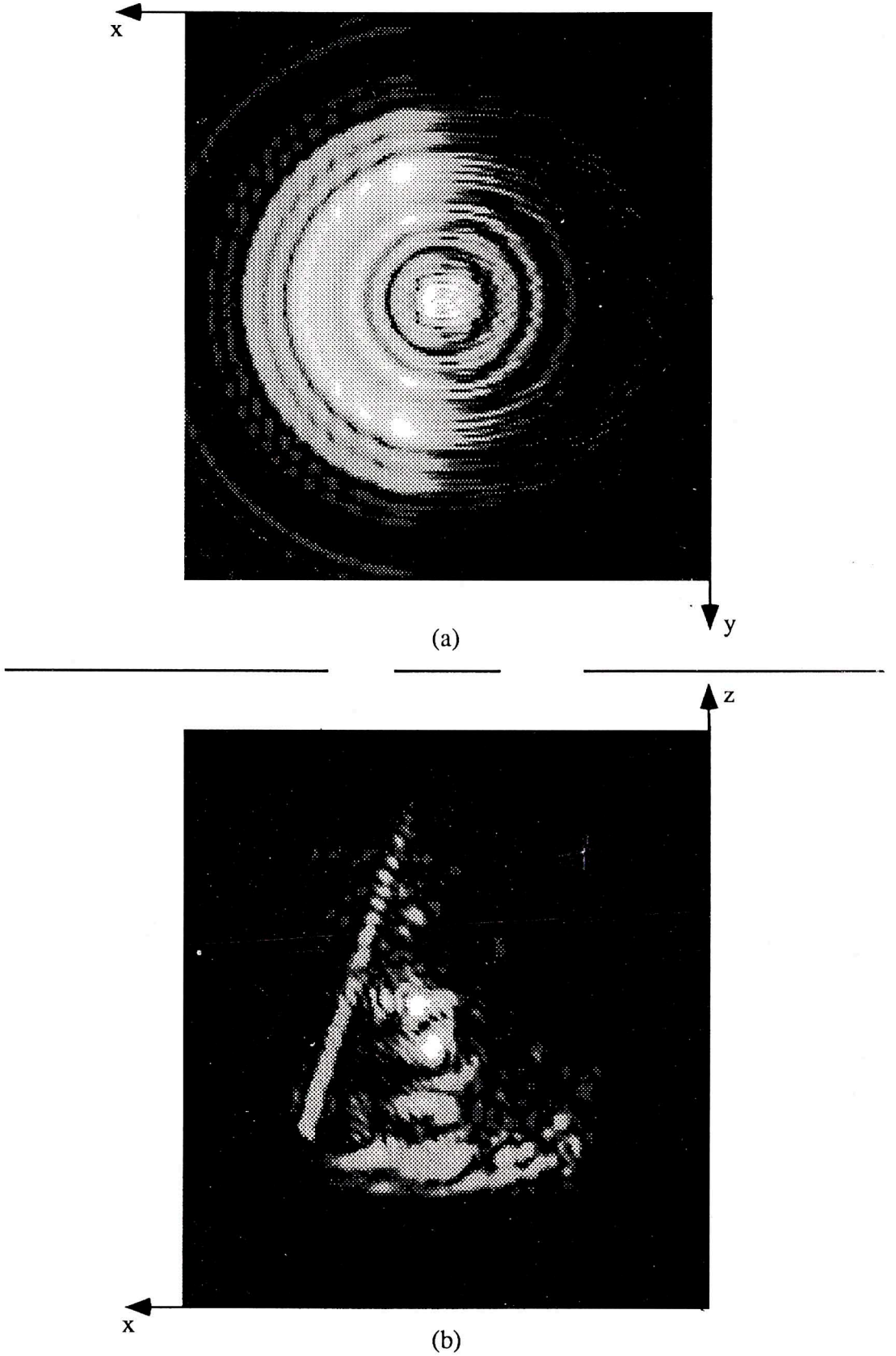

Fig. 17 - Projection plane images of the dielectric cone target obtained by processing the single azimuth sweep corresponding to forty-five degrees elevation, $\theta = 45°$.

CONCLUSION

Microwave holography has been presented as an alternative to the more conventional SAR and ISAR imaging radars [Farhat, 1981, Langenberg, 1987, Mensa, 1984, Munson, 1983]. Most of the work to date has concentrated on two-dimensional imaging, or three-dimensional imaging using tomographic techniques [DeVaney, 1981, Mensa, 1984]. Some experiments have been reported in the literature, but the projection images are of two-dimensions only [Farhat, 1981]. SAR imagers do not possess inherent three-dimensional imaging capability. ISAR imagers can produce resolution in three-dimensions provided object motion is sufficient in two of the dimensions. Holographic SAR requires no additional processing or data acquisition to provide for three-dimensional projection plane imaging. This capability is shown with the discrete target experiment reported in this paper. In addition to projection plane imaging, three-dimensional resolution is possible using tomographic processing with a true three-dimensional measurement set. Comparison of the two techniques is facilitated by the second experiment reported in this paper.

Both types of three-dimensional imagery have advantages and drawbacks. From a data acquisition point of view, the projection plane imaging process is the more efficient of the two techniques. This process requires only a single pass over the target to produce three-dimensional resolution. This advantage is important for remote sensing requiring airborne, or spaceborne platforms. The drawback to the technique is that each of the image planes formed from the data set will contain projections of all scattering sources comprising the target. To overcome this problem a full three-dimensional measurement is required. Tomographic processing can then be utilized to image specific planes of the scattering function. This is the most desirable technique for controlled experiment applications such as non-destructive testing or medicine.

REFERENCES

Chan, C. K. FARHAT, N. H. 1981, "Frequency Swept Tomographic Imaging of Three-Dimensional Perfectly Conducting Objects," IEEE Transactions on Antennas and Propagation, Ap-29, No. 2., 312.

Devaney, A. J., 1980, "A new approach to emission and transmission CT", 1980 Ultrasonics Symposium, 979.

Goodman, J. W., 1968, Introduction to Fourier Optics, (New York: McGraw-Hill).

Langenberg, K. J., 1987, Basic Methods of Tomography and Inverse Problems, Part II, (Bristol: Adam Hilger).

Mensa, D. L., 1984, High Resolution Radar Imaging, (California, Artech).

Munson, D. C., O'Brien, J. D., Jenkins, W. K., 1983, "A Tomographic Formulation of Spotlight-Mode Synthetic Aperture Radar", Proceedings IEEE,. 71, 917.

Radon, J., 1917, Uber die bestimmung von funktionen durch ihre intergralwere langs gewisser mannigfaltigkeiten, Berichte Saechsishe Akademie der Wissenschaften, 69, 262.

Ramachandran, G. N., Lakshminarayanan, A. V., 1971, Three-dimensional reconstruction from Radiographs and electron micrographs: application of convolutions instead of Fourier transforms, Proceedings of the National Academy of Science, USA,.69, 2236.

Schindel, R. F., 1989, Experimental Diverse Microwave Holography, Ph.D dissertation (Arlington).

Wang, Y.M., Chew, W. C., 1989, An iterative solution of the two-dimensional electromagnetic inverse scattering problem, International Journal of Imaging Systems and Technology, 1, (John Wiley and Sons, Inc.).

Wehner, D.R., 1987, High Resolution Radar, (MA, Artech).